ADVANCED ENGINEERING MATERIALS

COMMUNICATION

DOI: 10.1002/adem.200800329

Analysis of Anisotropic Void System in Electron-Beam Physical-Vapour-Deposited (EB-PVD) Thermal-Barrier Coatings**

By *Bilge Saruhan,* René Ochrombel, Vasyl Ryukhtin* and *Albrecht Wiedenmann*

Thermal barrier coatings (TBCs) are used as a viable additional method to air-cooling to decrease the inlet temperature and to protect turbine blades located at the high-pressure zone of aircraft engines and stationary gas turbines. Electron-beam physical vapour deposition (EB-PVD) is currently the most-accurate manufacturing process to produce lightweight coatings. Today state-of-the-art TBCs still consist of an yttria-stabilized zirconia (YSZ) top-coat, a metallic (Pt/Al or NiCoCrAlY) bond-coat (BC) and, between these two, a thermally grown oxide (TGO) based on Al_2O_3. The ceramic top-coat has to exhibit a low thermal conductivity and has high values of strain tolerance owing to its intrinsic columnar microstructure. The most-promising methods to fulfil this task and improve the efficiency in turbines are through optimizing the properties by tailoring the resulting zirconia phases and microstructure on the TBC.

The morphology and density of the columnar microstructure of EB-PVD TBCs can be varied by changing the deposition parameters, such as the chamber pressure, substrate temperature and rotation speed.[1–3] The morphology in EB-PVD YSZ TBCs contains individual columns growing on the substrate in a preferred crystallographic direction. Different kinds of pores in the microstructure influence the thermal conductivity according to their size, shape, orientation and volume.[4] These pores are divided into open (intercolumnar and secondary columnar porosity) and closed (intracolumnar porosity) pores. In particular, the porosity between the secondary columns (the so-called feather-arm features) in EB-PVD TBCs is recognized as an important factor controlling the thermal conductivity. Since most of the heat flows through the conducting columns and the in-plane thermal gradient does not vary across the parallel-aligned primary columns and intercolumnar gaps, it is considered that the intercolumnar gaps orientated parallel to the heat-flux induce only a slight effect on the thermal conductivity.[5–6]

Characterization of the pores in these coatings requires the employment of sophisticated techniques due to their sizes and size differences, accessibility (open and closed pores) and anisotropy. Use of innovative methods has been reported for the precise and detailed evaluation of open and closed porosity changes on ceramic materials during service-simulated conditions. These methods are based on the transmission of X-rays or neutrons through the coatings. Small-angle neutron scattering (SANS) represents, with some advantages, an alternative to the gas-adsorption methods. This method is sensitive to both closed and open porosities and, in many cases, offers a more-complete analysis of the measured porosity.[7] SANS has already been applied to study the processing-microstructure relations and sintering of EB-PVD and air-plasma-spraying (APS) coatings.[8–15] These studies, in particular, focused on the measurement of the Porod scattering,[16,17] derived from the terminal slope in the SANS spectra, to determine the characteristics of voids in the porous materials. The quantitative information obtained on the corresponding interface surface area is dominated by the measured intensities. Since the fine features in the microstructure are the major contributors to the deduced area,[11a–b] it is important to measure the minimum size of the scatterers present in a material in order to ascertain the origin of the scattered apparent Porod surface area. The Porod scattering technique does not require a void-shape model, and thus, is especially useful for studies of void systems with complex shapes.[8]

This study reports processing-related morphological differences that yield three different EB-PVD Partially Yttria Stabilized Zirconium (PYSZ) coatings, whose thermally activated changes are analysed by employing a matching-mixture immersion and in situ high-temperature small-angle neutron scattering (SANS) techniques. The total surface area,

[*] *Dr. B. Saruhan, Dr. R. Ochrombel*
German Aerospace Centre, Institute of Materials Research
D-51147 Cologne, Germany
E-mail: bilge.saruhan@dlr.de
Dr. V. Ryukhtin
Technical University of Berlin
Str. des 17. Juni 135, D-10623 Berlin, Germany
Dr. A. Wiedenmann
Institute Laue-Langevin
Grenoble, France

[**] *The authors acknowledge the assistance of C. Kröder, J. Brien, D. Peters and A. Handwerk of DLR for the careful production of the coatings. We also acknowledge the support of Mr. W. Schönau from DLR for LFA measurements and the intensive support of Dr. D. Wallacher from Helmholtz Center for Materials and Energy during the SANS measurements. We thank Dr. A. Flores Renteria for providing the SEM micrographs and also for his preliminary work on this subject, which provided us a valuable basis.*

pore size and pore morphology, as well as anisotropic changes are determined in detail and these are correlated with thermally induced deviations in the thermal conductivity.

Experimental Methods

Processing of Coatings and Sample Preparation

EB-PVD coatings were produced by employing ''von Ardenne'' pilot-plant equipment with a maximum EB power of 150 kW. Evaporation was carried out from single source (ingot) that had the standard chemical composition (7–8 wt % Y_2O_3-stabilized ZrO_2) with a diameter of 62.5 mm and a length of 150 mm. The vapour phase was deposited on plane substrates under three different rotating modes by mounting the substrate in a holder with its axis perpendicular to the evaporation source. The ceramic-substrate temperature was varied between 850 °C and 1000 °C at rotation speeds of 3, 12, and 30 rpm to yield different deposition rates. A thickness of approximately 400 μm was achieved by the EB-PVD coating of PYSZ directly on FeCrAl-alloy substrates (12.7 mm diameter) without a bond coat. Since the applied analysis methods (SANS and laser-flash analysis (LFA)) require the use of coatings in free-standing conditions, the substrates were etched out completely in an acid solution to obtain the free-standing coatings. Subsequently, the corresponding specimens were heated to 1100 °C at a heating rate of 5 °C min^{-1} and isothermally aged at this temperature in air for 1 h and 100 h. After the respective isothermal ageing, the samples were removed from the furnace and ''quenched'' in air to freeze the microstructure.

Methods of Characterization

Measurement of Thermal Conductivity by Laser Flash Analysis (LFA)

The thermal conductivity of the PYSZ samples was measured using the laser-flash method (LFA 427, NETZSCH, Germany). Because this method is described extensively in the literature, only a brief description will be given here. In the laser-flash technique a disc-shaped specimen positioned in a furnace is heated to the desired temperature. Additionally, the specimen is heated homogenously through the adsorption of energy from a short, highly energized laser impulse. The heat generated at the front surface fluxes through the specimen to the rear side. An IR detector measures the signal. The thermal diffusivity is determined from the measured temperature rise as a function of time.

The disc-shaped specimens had a diameter of 12.7 mm. All of the laser-flash experiments in the present work were performed in vacuum, both on heating and subsequent cooling between room temperature and 1000 °C at intervals of 100 °C. Usually, three measurements were made at each temperature setting. The individual data sets were averaged for further evaluation.

Analysis of Laser-Flash Experiments

Temperature rise as a function of time was analysed using the program provided by NETZSCH, according to the relationship described in Equation (1).

$$\frac{\partial T}{\partial t} = \alpha\left(\frac{\partial^2 T}{\partial x^2} + \frac{\partial^2 T}{\partial r^2} + \frac{1}{r}\frac{\partial T}{\partial r}\right) \quad (1)$$

For analysing the measurements, the two-dimensional heat model was used, solved by Cape and Lehman,[18] including a radiation correction. This model is valid for materials exhibiting homogenous thermal diffusivity or only marginal differences in its tensor components. The thermal conductivity, λ_{ij}, of the coatings was calculated using Equation (2).

$$\lambda_{ij} = c_p \cdot \rho \cdot \alpha_{ij} \quad (2)$$

In Equation (2), ρ represents the density, c_p the specific heat and α_{ij} the thermal diffusivity.

The specific heat, c_p, for the PYSZ was measured by differential scanning calorimetry (DSC) (NETZSCH DIAMOND). Our measurements are in good agreement with the literature data from Touloukian,[19] measured for pure zirconium dioxide. Thereby, different phases of PYSZ that only show marginal differences in the specific heat can be expressed by the empirical formula given in Equation (3), which is valid in the temperature range T from 300 to 1200 K, and where the units of c_p are J g^{-1} K^{-1}.

$$c_p = -68.580/T + 0.6856 \quad (3)$$

Investigation of Coating Morphology and Microstructure

The microstructure of the cross sections and at the coating tips was characterized visually using a field-emission scanning electron microscope (FE-SEM) (LEITZ LEO 982, Germany). Since the columnar microstructure of these coatings contains open (intercolumnar gaps and voids between feather-arms) and closed (intercolumnar pores) porosities, it was necessary to use such measurement methods that are capable of tracking the surface-area changes of all of the types of pores, in addition to the microstructural characterization.

Small-Angle Neutron Scattering (SANS)

This study focuses on the measurement and characterisation of voids in a porous material. Small angle neutron scattering (SANS) is especially useful for studies of void systems with complex shapes. This analysis method is sensitive to both opened and closed porosities. This instrument covers a Q range from $\sim 2 \times 10^{-4}$ Å^{-1} to 2×10^{-2} Å^{-1}, which approximately corresponds to a size range of about 0.1–3 μm. The wavelength was 2.06 Å. The samples were installed perpendicularly to the neutron beam, and were of cross section 3 × 2 mm. The samples were fixed in quartz cells and were filled with mixture of heavy and light water (89/11 in wt %) after the first round of measurements. The scattering-length density (SLD) of this mixture was equal to the empirical SLD value of 7 wt % PYSZ (5.46×10^{10} cm^{-2}).

COMMUNICATION

The high-temperature and matching point SANS experiments were performed using a V-4 SANS instrument at the Helmholtz Center for Materials and Energy in Berlin. The sample-to-detector distance was variable between 1 and 16 m. A detailed description of the measurement configuration is given in reference.[14] The samples were placed in a sample holder using a cadmium mask with a circular slit with a diameter of 6 mm. Under measurement conditions, the irradiated volume of the specimens was about $113\,mm^2 \times 0.4\,mm$.

The scattered neutron intensity, $I(Q)$, was measured using an incident beam along the plane perpendicular to the substrate's plane (parallel to the column axis) over two sample–detector distances: 1 m and 4 m, employing a neutron wavelength of $\lambda = 0.605$ nm. The obtained data were corrected for background scattering, transmission and detector efficiency, and normalized to absolute units by using water as the calibration-standard procedure. Quantitative information of the surface area corresponding to the intracolumnar pores was achieved in the form of the corresponding Porod constant (P_c) as a function of the azimuthal angle by converting the 2D data to 1D scattering profiles averaged over 5°. The Porod constant (P_c) is directly proportional to the apparent Porod surface area (S_v) according to Equation (4):

$$S_v = \frac{P_c}{2\pi|\Delta\rho|^2} \tag{4}$$

In Equation (4), $\Delta\rho$ is the contrast in scattering length density between the pores and the PYSZ material. In this method, the measured Porod scattering intensity, $I(Q)$, is linearly proportional to the interfacial surface-area projection in a plane perpendicular to the scattering vector, Q, corresponding to dimensions measured parallel to it.[16]

In view of the fact that the Porod scattering measured in one direction does not reflect the total surface area of the scatterers but a projection in the plane perpendicular to the scattering vector Q, it is often called the apparent Porod surface area, which can be calculated from its corresponding Porod constant by Equation (3). The total specific area of the scatterers within the sample can be obtained from the apparent Porod constant by averaging over all 3D directions in the material.[20] However, this apparent surface area is useful to analyze the microstructural changes between the samples by measuring them under the same conditions.

The in situ high-temperature SANS technique has been employed to study the thermally activated pore and porosity changes. In an effort to separate the scattering from the open and closed porosities, an experimental trick was used by filling the pores with liquid (D_2O/H_2O) with the same value of scattering, which is called a matching-mixture experiment.

Results and Discussion

Figure 1 shows SEM micrographs of the investigated EB-PVD PYSZ top-coats having morphological differences in their column diameter, in the size and shape of the intercolumnar gaps and of the voids between feather-arm features. These differences were produced by altering the process parameters during the EB-PVD coating, as specified in Table 1. The morphologies were designated according to their appearances on the micrographs.

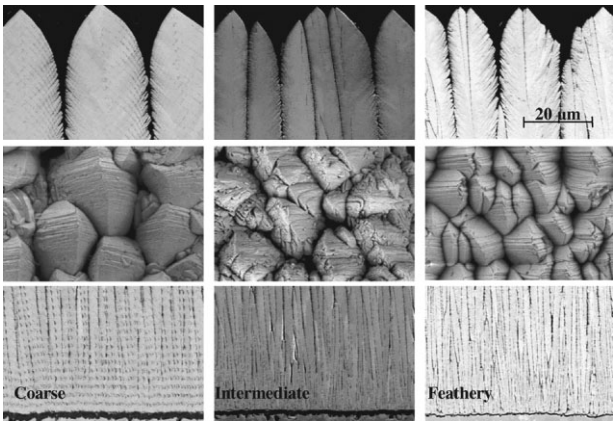

Fig. 1. Scanning electron micrographs of as-coated EB-PVD PYSZ-TBCs having three different morphologies: ''coarse'', ''intermediate'' and ''feathery'' (top row), in cross section, perpendicular to the rotation axis, (middle row) from the coating tip and (bottom row) morphology at the substiate side of the coating.

During the EB-PVD process of the coatings, quasisingle crystalline columns with a very-fine diameter (2–3 μm) start to grow on the substrate surface, enlarging their diameter (10–20 μm) and achieving pyramidal shapes at the coating tip. These columns are only weakly interconnected to each other, displaying intercolumnar gaps, which accounts for the high open porosity. The gaps between the primary columns are a few nanometers (nm) at the substrate side of the coatings and can be as large as 1 μm at the tip of the coating.

The three analysed coatings display the typical columnar EB-PVD PYSZ with evident differences in the column diameter as well as significant variations in the gaps between the feather-arms and intracolumnar features situated at the rotation path within the columns. The ''intermediate'' microstructure, which was produced under a rotation speed of 12 rpm, shows symmetrical columns reaching a diameter of approximately 10 μm at the tip zone of the coating (bulk density $= 4.37\,g\ cm^{-3} \pm 3\%$). The so-called feather-arm features surrounding the columns are elongated and extend from the column edge to the column axis with an angle of approximately 45° (see Fig. 2a). The ''coarse'' microstructure is characterised by larger column diameters and the ''feathery'' microstructure consists of more-defined feather-arm features.

Table 1. The process parameters during the EB-PVD coating.

Morphology	Chamber Pressure [mbar]	Substrate Temperature [°C]	Rotation Speed [rpm]
Coarse	8×10^{-3}	1000	3
Intermediate	8×10^{-3}	950	12
Feathery	8×10^{-3}	850	30

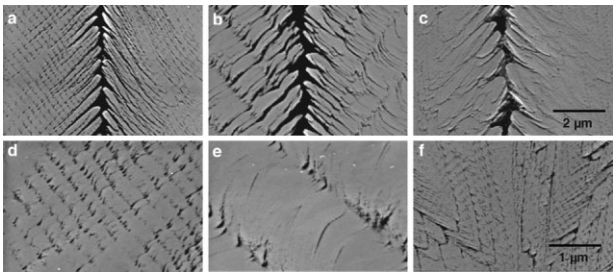

Fig. 2. Scanning electron micrographs of cross sections perpendicular to the rotation axis for the three different EB-PVD morphologies of the PYSZ-TBCs, showing the intercolumnar pores and the pores between the feather-arms in the as-coated condition: a,d) ''intermediate''; b,e) ''feathery''; c,f) ''coarse''.

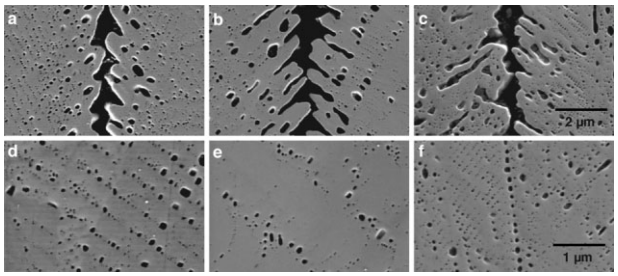

Fig. 3. Thermally induced configuration of the gaps between feather arms: a) ''intermediate'', b) ''coarse'', and c) ''feathery''; and the intracolumnar pores: d) ''intermediate'', e) ''coarse'', and f) ''feathery'', of the three analysed EB-PVD PYSZ-TBCs in aged conditions (1100 °C for 100 h).

Although the EB-PVD PYSZ coatings show a columnar structure that is grown in a preferred crystallographic direction, attention must be paid to the differences concerning open (intercolumnar gaps) voids between feather-arms and closed porosity (intracolumnar pores). As the middle row of Figure 1 demonstrates, the EB-PVD PYSZ TBCs with the ''coarse'' morphology show columnar diameter sizes as large as 20 μm, which is nearly double the size of those with the ''intermediate'' or ''feathery'' morphologies. On the other hand, the detailed investigation of the microstructures shown in Figure 2b and 2e reveals that the feathery TBCs, deposited by employing the highest rotation speed of 30 rpm, contain a higher open porosity, generated from voids that present in sizes smaller than 1 μm between the secondary columns and extend in lenth inside the columnar structure. The ''coarse'' microstructure was produced by employing a higher substrate temperature combined with the slowest rotation speed (3 rpm) and displays broader intercolumnar gaps (Fig. 2c and 2f). In the case of the ''intermediate'' and ''coarse'' microstructures, larger intracolumnar pores are anticipated to form, due to the applied lower rotation speeds (12 and 3 rpm, respectively) during processing. Moreover, since they are manufactured at higher substrate temperatures, only a fraction of the pores are able to continue to grow at each rotation phase and survive until the next array of new pores are created.

Thermal treatment of the coatings at 1100 °C for 100 h leads to closure of this porosity. As presented in Figure 3, the EB-PVD-manufactured PYSZ coatings show different sintering behaviours resulting in different morphological development. After heat treatment at 1100 °C for 100 h, the sintering process becomes active, leading to morphological changes resulting in mass transfer through bridging at the contact points between the primary and secondary columns. This phenomenon is enhanced at the bottom (foot) zone of the coating. The columns, which were initially interrupted from growing throughout the coating thickness, tend to pull together and create finer channels between them. At the same time, significant thermally induced changes occur at the finer feather-arm regions and intracolumnar pores.

In order to enable a quantitative analysis of the porosity, the SANS measurements were carried out. The raw SANS data of the as-coated and heat-treated EB-PVD PYSZ with ''intermediate'' and ''feathery'' morphologies are shown in Figure 4. These data were obtained using a V-4 SANS instrument at a wavelength of 6.05 Å. 2D data were corrected for background scattering and transmission. The presented 1D curves were obtained by radial averaging.

The SANS data from the coatings that were heat-treated in air (sintered) and in vacuum (furnaced) are quite similar. Similar scattering behaviour was observed for coatings with the ''feathery'' morphology measured in the matching liquid (see Fig. 4d). Similar to the as-coated coatings, not much difference is observed for the coatings that were heat-treated in air and in vacuum, indicating that the closed porosity of these coatings has a similar microstructure under these conditions. However, the microstructure of the closed porosity in the EB-PVD PYSZ TBC with the ''intermediate''

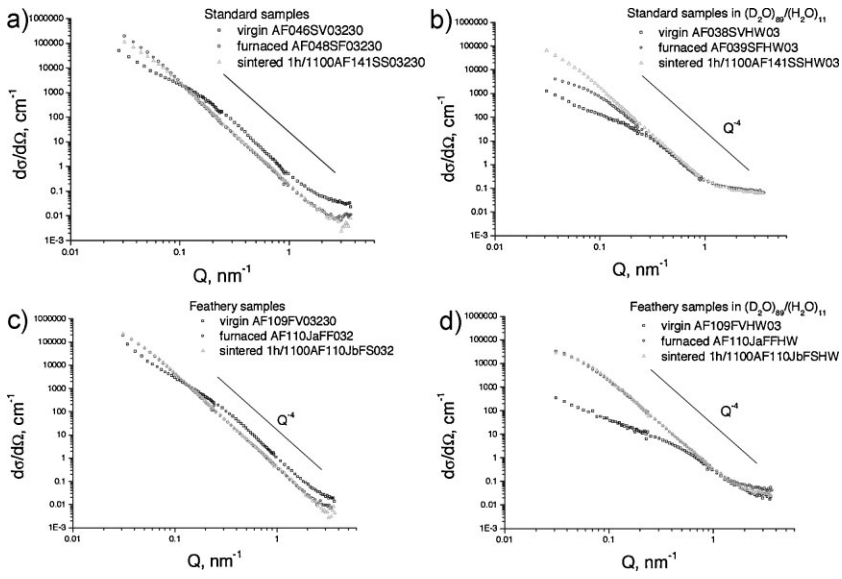

Fig. 4. 1D SANS scattering functions (averaged radially) of: a,b) intermediate; and c,d) feathery types of samples, obtained in as-coated coatings without any processing (a,c), and in a matching mixture of heavy and light water (b,d).

morphology depends strongly on the type of atmosphere present during sintering. In particular, the deviation between the scattering data for the samples sintered in air and under vacuum can be seen in the region of small Q values ($<0.3\,nm^{-1}$), which corresponds to larger pores (see Fig. 4b).

The apparent Porod constant was used for quantitative comparison of the microporosity in the investigated TBCs. In the case of the isotropic microstructure, the Porod constant is proportional to the specific surface (S/V). To obtain the true Porod constant for the anisotropic structure, 3D analysis must be done. However, the apparent Porod constant can be used for describing changes at the porosity surface. The fitting procedure was applied to the high-Q region of the scattering curves obeying the Porod law ($\sim Q^{-4}$).

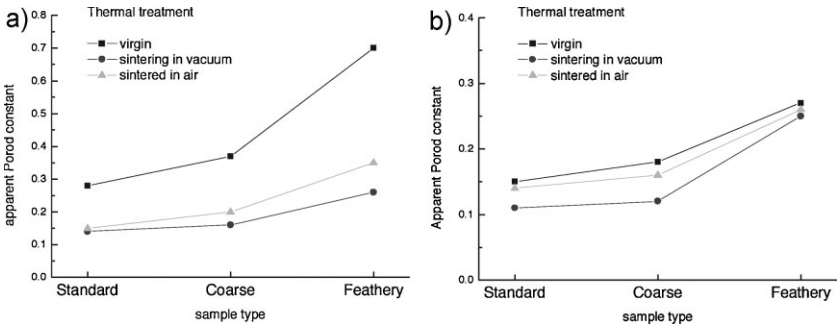

Fig. 5. Specific surface values for three types of sample obtained by SANS on measuring in a) air and in b) the mixture of heavy and light water (89/11 wt %).

The total (closed and opened) bulk porosity contributes to the measured SANS functions that are shown in Figure 4a–c. In order to differentiate between these two porosity types, the samples were measured once in as-coated conditions without any processing (Fig. 4a and 4c) and then immersed in a matching mixture of D_2O/H_2O (89/11 wt %) (see Fig. 5).

Figure 5 indicates that the values of the Porod constant for the total porosity decrease, for all of the investigated coatings, several times after sintering. This is likely to be due to the morphological changes that occur at the pores, which became smoother, the smaller ones becoming more isotropic. Such changes in the anisotropy have already been observed with similar TBCs, as reported in ref. [18]. The decrease of the apparent Porod constant for the closed porosity is not that great (see Fig. 5b). For samples with the ''intermediate'' (e.g., standard) and ''coarse'' morphologies, the decrease of this parameter is larger for the coatings sintered in air than for those heat-treated in vacuum.

The Porod constant of the coatings measured without any processing indicates a change in the total porosity. The parameter is greatly decreased for the coating designated as ''feathery'' after sintering (Fig. 5a). Its counterpart, obtained in the matching mixture, in turn, does not show much difference, pointing out the occurrence of no or very little change in the closed porosity of this coating type (Fig. 5b). This explains why, in the coating with the ''feathery'' morphology, most of the porosity change occurs in the open porosity after sintering in air and under vacuum.

The fitted Porod parameters in all of the investigated coatings sintered in air are lower in comparison with those sintered under vacuum. This may be caused by the additional gas pressure present in the case of heat treatment in air ($\sim$1 bar) leading to lower volume fractions for the total porosity. However, the morphology (smoothness and anisotropy) must be the same for the particular type of TBC, independent of the sintering environment.

The obtained high-temperature SANS data was fitted using a model that applies a revolution of the oriented ellipsoids by means of fitting program SAS profit. The aspect ratio of the ellipsoids (R/r) is shown in Figure 6a–b for the coatings designated as ''intermediate'' and ''coarse'', respectively. For both coatings, the aspect ratio remains almost constant up to 900 °C and starts to decrease at about 1000 °C.

At the same time, the specific surface decreases with temperature, as revealed by fitting the high-temperature SANS data (see Fig. 7a–b). Figure 7a–b also indicates that the surface-area decrease is caused by thermal expansion within the coatings, as well as by sintering starting at temperatures above 900 °C. These parameters are obtained only by measuring during heating and on cooling under vacuum. The differences in the specific surface before heating and after cooling are larger in the coatings with the ''coarse'' morphology.

These results indicate that the changes in the surface area start to occur already at temperatures lower than 600 °C, although the pore-morphology changes may take place at relatively higher temperatures and account for a more-substantial amount of the surface-area reduction above 800 °C for the coatings with the ''intermediate'' morphology than for those with ''coarse'' morphology.

Moreover, the combination of the matching-mixture immersion and high-temperature SANS fitting methods indicates that after heat-treatment at 1100 °C for 1 h, the

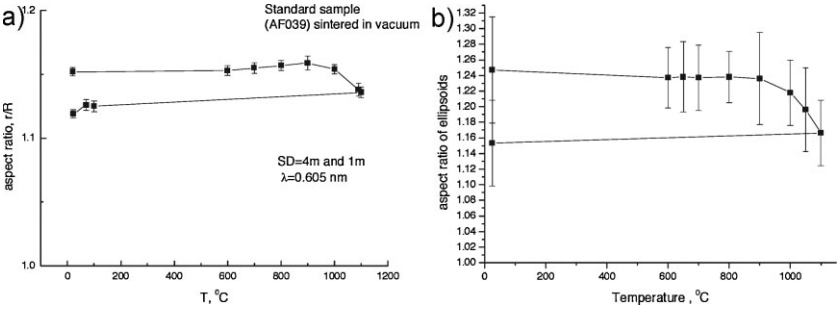

Fig. 6. Aspect ratio of the ellipsoids used for the fitting of the high-temperature SANS data of: a) the coatings (standard) with intermediate morphology, and b) the coatings with coarse morphology.

ADVANCED ENGINEERING MATERIALS

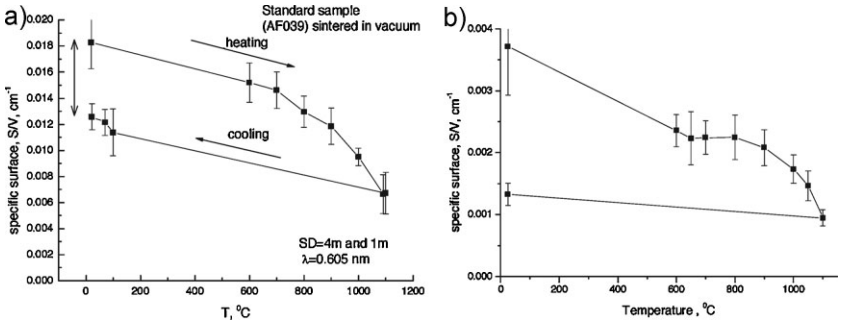

Fig. 7. Calculated specific surface area obtained after fitting the high-temperature SANS data from the coating with (a) "intermediate" and (b) "coarse morphology"

proportions of the closed and open porosity change, since the total porosity remains almost constant.

The thermal conductivity of the coatings was analysed before and after ageing. There are clear differences in the thermal-conductivity values of the three, as-coated morphologies. Figure 8 shows the change in the thermal conductivity of the EB-PVD PYSZ coatings as a function of temperature, dependent on the processing and the treatment state and conditions. The thermal conductivity of an untreated coating, regardless of morphology, is lower than those that were heat-treated in air. It is obvious that the EB-PVD PYSZ coatings with the ''feathery'' morphology have a significantly lower thermal conductivity than those with other morphologies. This is primarily due to the higher open porosity and the resulting lower bulk density. The rise of the conductivity is mostly influenced by the change in porosity. Typical thermal-conductivity values for the EB-PVD PYSZ coatings with the ''feathery'' morphology are around 1.1 W (mK) $^{-1}$. The surface temperatures of turbine blades in current aircraft engines are around 1100 °C. Thermal ageing in air at 1100 °C for 100 h leads to an increase of thermal conductivity of nearly 1.5 W (mK) $^{-1}$. The thermal conductivity of thermally aged ''feathery'' coatings is still lower than that of thermally untreated EB-PVD PYSZ coatings with the ''coarse'' morphology.

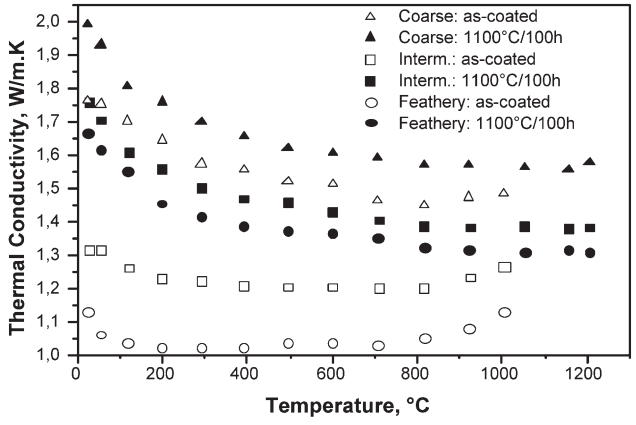

Fig. 8. Thermal-conductivity values of the three investigated coating morphologies (feathery, intermediate and coarse) as a function of measuring temperature in the as-coated condition and after heat treatment at 1100 °C for 100 h.

There are noticeable increases in the thermal conductivity of the investigated coatings after heat treatment. Assuming that the intercolumnar pores orientated parallel to the heat flux induce only a slight effect on the thermal conductivity of EB-PVD TBCs, these differences can principally be related to the thermally induced changes of the voids between the feather-arms and the intracolumnar pores. Although the coatings with the ''intermediate'' morphology show the highest thermal-conductivity increase, the total surface-area reduction is not the highest. Thus, it is more likely that the changes in pore shape have more influence on the thermal conductivity than the reduction of the surface area.

In summary, a fast rotation and a low substrate temperature leads to the formation of high-aspect-ratio feather-arms, a long and elongated curved shape of the intracolumnar pores and highly populated pore arrays. Such a microstructure yields a very-low thermal conductivity. Although it may suffer under thermal ageing, which results in a reduction of the surface area, the formation of new closed pores with elongated shapes, located perpendicular to the heat-flux, leads to less of an increase in the thermal conductivity. The EB-PVD PYSZ TBC with large columns and fewer feather-arm features has the highest thermal conductivity. These types of feature may result in lower surface-area changes at elevated temperatures; however, the small and isotropic intracolumnar pores do not interrupt the heat-flux, resulting in higher thermal-conductivity values.

Conclusions

EB-PVD PYSZ TBCs with different morphologies and microstructures were produced by varying the parameters of the EB-PVD process, principally the substrate temperature and the rotation speed.

Significant differences in the thermal conductivity of the resulting three morphologies are measured. These are related to the volume of open and closed porosity and their morphologies. The thermal conductivity is very sensitive to thermally activated changes that occur in these features due to the resulting sintering processes. The general trend can be listed as following:

a) Isotropic small pores are less effective in reducing thermal conductivity;
b) Elongated pores withstand sintering and may remain anisotropic, even though a total, high surface-area reduction occurs;
c) A closed porosity can be as effective as an open porosity in reducing thermal conductivity, as long as the configuration relative to the heat-flux is correct;

d) Highly populated intracolumnar pore arrays are more resistive to thermal-conductivity increases and provide the lowest thermal conductivity.

Received: September 30, 2008
Final Version: January 12, 2009
Published online: May 12, 2009

[1] U. Schulz, J. Münzer, U. Kaden, *Ceram. Eng. Sci. Proc.* **2002**, *23*, 353.
[2] U. Schulz, K. Fritscher, C. Leyens, M. Peters, W. A. Kaysser, *Materialwissenschaft Werkstofftechnik* **1997**, *28*, 370.
[3] K. Wada, N. Yamaguchi, H, Matsubara, *Surf. Coating Technol.* **2005**, *191*, 367.
[4] J. R. Nicholls, K. J. Lawson, A. Johnstone, D. S. Rickerby, *Surf. Coat. Technol.* **2002**, *151–152*, 383.
[5] D. D. Hass, A. J. Slifka, H. N. G. Wadley, *Acta Materialia* **2001**, *49*, 973.
[6] U. Schulz, B. Saruhan, K. Fritscher, C. Leyens, *Int. J. Appl. Ceram. Technol.* **2004**, *1*, 302.
[7] P. J. Hall, S. Brown, J. Fernandez, J. M. Calo, *Carbon* **2000**, *38*, 1257.
[8] J. Ilavsky, A. J. Allen, G. G. Long, *J. Mater. Sci.* **1997**, *32*, 3407.
[9] J. Ilavsky, A. J. Allen, G. G. Long, S. Krueger, *J. Am. Ceram. Soc.* **1997**, *80*, 733.
[10] J. Ilavsky, G. G. Long, A. J. Allen, C. C. Berndt, *Mater. Sci. Eng. A* **1999**, *272*, 215.
[11] a) A. Kulkarni, Z. Wang, T. Nakamura, S. Sampath, A. Goland, H. Herman, J. Allen, J. Ilavsky, G. Long, J. Frahm, R. W. Steinbrech, *Acta Materialia* **2003**, *51*, 2457. b) Z. Wang, A. Kulkarni, S. Deshpande, T. Nakamura, H. Herman, *Acta Materialia* **2003**, *51*, 5319.
[12] A. J. Allen, G. G. Long, H. Boukari, J. Ilavsky, A. Kulkarni, S. Sampath, H. Herman, A. N. Goland, *Surf. Coating Technol.* **2001**, *146–147*, 544.
[13] A. Flores Renteria, *Dissertation*, Fakultät für Georessourcen und Materialtechnik RWTH Aachen (Aachen), **2006**.
[14] A. Flores Renteria, B. Saruhan, J. Ilavsky, in *Advanced Ceramic Coatings and Interfaces (Ceramic Engineering & Science Proceedings)*, Vol. *27(3)* (Eds: A. Wereszczak, E. Lara-Curzio, D. Zhu), John Wiley & Sons. Inc., Hoboken NJ **2007**, p. 3–16.
[15] A. Flores Renteria, B. Saruhan, U. Schulz, H.-J. Raetzer-Scheibe, J. Haug, A. Wiedenmann, *Surf. Coat. Technol.* **2006**, *201*, 2611.
[16] G. Porod, in *Small-Angle X-ray Scattering* (Eds: O. Galtter, O. Kratky), Academic Press, London UK **1982**, p. 17–51.
[17] J. Haug, A. Wiedenmann, A. Flores, B. Saruhan-Brings, P. Strunz, *J. Phys. B* **2006**, *385–386*, 617.
[18] J. A. Cape, G. W. Lehman, *J. Appl. Phys.* **1963**, *34*, **1909**.
[19] Y. S. Touloukian, E. H. Buyco, Specific Heat-Nonmetallic Solids, in *Thermophysical Properties of Matter*, Vol. *5*, IFI/Plenum, New York-Washington **1970**, p. 293–295.
[20] T. Keller, W. Wagner, N. Margadant, S. Siegmann, J. Ilavsky, J. Pisacka, Brno, Czech Republic **2001**, 460–468.

